International Journal of Microwave and Wireless Technologies, 2013, 5(2), 141–148.
doi:10.1017/S1759078713000068

INDUSTRIAL AND ENGINEERING PAPER

A multi-harmonic model taking into account coupling effects of long- and short-term memory in SSPAs

CHRISTOPHE MAZIERE[1], EMMANUEL GATARD[1], CEDRIC ENGUEHARD[1] AND BJORN GUSTAVSEN[2]

This paper presents a new macro modeling methodology for solid-state power amplifiers (SSPAs) and packaged transistors used in communication systems. The model topology is based on the principle of harmonic superposition recently introduced by Agilent Technologies' X-parameters™ combined with dynamic Volterra theory. The resulting multi-harmonic bilateral model takes into account the coupling effects of both short- and long-term memory in SSPAs. In this work, the behavioral model was developed from time-domain load pull and used to simulate the amplifier's response to a 16-QAM signal with specific regards to ACPR and IM3.

Keywords: Power amplifiers and linearizers, Linear and nonlinear CAD techniques

Received 30 September 2012; Revised 9 January 2013; first published online 18 February 2013

I. INTRODUCTION

In modern communication systems, solid-state power amplifiers (SSPAs) are one of the most critical components for consideration as they consume a large portion of DC. Because of this, accurate amplifier behavioral models are needed in order to establish accurate link budget estimates used in system optimization. An efficient "black-box" model must be able to accurately determine the nonlinear dispersive effects (memory effects) without requiring massive amounts of computational resources.

Several approaches have been taken to accomplish the tasks at hand. A first and reasonable approach focuses on the memory-effect impact on amplifier bandwidth. Parallel and/or series associations of linear filters and memoryless nonlinearities were reported in [1–4]. The principle drawback of such models is that they cannot take into account the long-term memory effects caused by self-heating and low-frequency transient phenomena. Such effects occur in the bias circuitry when the injected RF signal is modulated. Furthermore, the extraction of such models may require a cumbersome optimization procedure where uniqueness of the solution is questionable. Alternatively, SSPA behavioral models, based on direct Volterra series expansion and digital filter representation adopted in [5–7], often lead to complex model architecture and optimization procedures. The combination of first-order modified Volterra series expansions reported in [8–10] enable a relatively straightforward extraction methodology with a good prediction of short- and long-term memory effects.

X-parameters™, Agilent Technologies' commercialization of the poly-harmonic distortion (PHD) nonlinear behavioral model [11, 12] can be interpreted as the natural extension of S-parameters to nonlinear operating conditions. In general terms, X-parameters involve the linearization of a dynamic spectral map dealing with the large signal operating conditions determined by both DC and RF spectral lines. The capabilities of X-parameter models applied to the simulation of cascaded nonlinear systems has been demonstrated in [11] for low-mismatched conditions. In [13] authors present an enhanced method of including long-term memory effects inside the X-parameter behavioral model in order to allow fast and precise simulation of narrow-band applications.

In this paper, an extension of the MHV (multi-harmonic Volterra) model presented in [14] is proposed. The extended MHV model combines the advantages of both the modified Volterra series and X-parameters models into a first order dynamic spectral map. The objective is to predict the influence of memory effects using in-band signals without losing harmonic content. Each nonlinear parameter of [11] is defined as a first order Volterra kernel. Compared with [13], the target is to model the coupling effect of long- and short-term dynamics in order to achieve a good prediction of performance in wideband applications. The extraction procedure is directly based on X-parameters methodology, using measurement post-processing or simulated data. The model equation is presented, as well as the extraction methodology. Simulation results which highlight the validity of the model are shown and compared with experimental data.

[1]AMCAD Engineering, 1 Avenue d'Ester, 87069 Limoges, France
[2]SINTEF Energy Research, N-7465 Trondheim, Norway
Corresponding author:
C. Mazière
Email: maziere@amcad-engineering.fr

II. MODEL TOPOLOGY

Consider a nonlinear device which suffers from memory effects, with the incident and scattered waves $a_i(t)$, $b_i(t)$ corresponding to the incident and reflected power waves on port numbers $i = 1,2$.

The output wave $b_i(t)$ can be expressed as a sum of fundamental and harmonic modulated tones (1):

$$b_i(t) = \mathrm{Re}\left\{\sum_{k=0}^{N} \tilde{b}_{ik}(t) e^{j2\pi k f_0 t}\right\}. \quad (1)$$

The general equation of a nonlinear system without memory maps the entire set of incident waves in envelope domain as (2)

$$\tilde{b}_{ik}(t) = f_{\mathrm{NL}}\begin{pmatrix} \tilde{a}_{11}(t), \tilde{a}_{12}(t), \tilde{a}_{13}(t), \ldots \\ \tilde{a}_{21}(t), \tilde{a}_{22}(t), \tilde{a}_{23}(t), \ldots \\ \tilde{a}^*_{11}(t), \tilde{a}^*_{12}(t), \tilde{a}^*_{13}(t), \ldots \\ \tilde{a}^*_{21}(t), \tilde{a}^*_{22}(t), \tilde{a}^*_{23}(t), \ldots \end{pmatrix}. \quad (2)$$

Assuming that the main nonlinearity is driven by the incident power wave $a_{11(t)}$ at the fundamental frequency, harmonic superposition can be applied to (2), resulting in a relationship governing two-port nonlinear systems (Fig. 1):

$$\tilde{b}^{ST}_{ik}(t) = \sum_{jl} S_{ik,jl}(|\tilde{a}_{11}(t)|) P^{k-l} \tilde{a}_{jl}(t) + \sum_{jl} T_{ik,jl}(|\tilde{a}_{11}(t)|) P^{k+l} \tilde{a}_{jl}*(t) \text{ with } P = e^{j\varphi_{\tilde{a}_{11}}(t)}. \quad (3)$$

However, the terms $S_{ik,jl}$ and $T_{ik,jl}$ are described by the incident wave a_{11} under steady-state conditions not taking into account memory effects. By using a discrete description with memory duration $T_m = M\Delta t$.

(Δt corresponds to the sampling step), equation (3) can be rewritten as

$$\tilde{b}_{ik}(t) = f_{\mathrm{NL}}\begin{pmatrix} \tilde{a}_{11}(t_{n-M}), \tilde{a}_{12}(t_{n-M}), \tilde{a}_{13}(t_{n-M}), \ldots \\ \tilde{a}_{21}(t_{n-M}), \tilde{a}_{22}(t_{n-M}), \tilde{a}_{23}(t_{n-M}), \ldots \\ \tilde{a}^*_{11}(t_{n-M}), \tilde{a}^*_{12}(t_{n-M}), \tilde{a}^*_{13}(t_{n-M}), \ldots \\ \tilde{a}^*_{21}(t_{n-M}), \tilde{a}^*_{22}(t_{n-M}), \tilde{a}^*_{23}(t_{n-M}), \ldots \end{pmatrix}. \quad (4)$$

In order to formalize the general equation (4), a dynamic Volterra-series expansion of the $S_{ik,jl}$ and $T_{ik,jl}$ terms of (3) is performed and results in

$$\tilde{b}_{ik}(t) = \sum_{jl} \begin{Bmatrix} S_{ik,jl}(|\tilde{a}_{11}(t)|) \times P^{k-l} \times \tilde{a}_{jl}(\Omega) \\ + \frac{1}{2\pi}\int_{-\infty}^{+\infty} H^{ST}_{ik,jl}(|\tilde{a}_{11}(t)|, \Omega) \times \tilde{a}_{jl}(\Omega) \times d\Omega \\ + \frac{1}{2\pi}\int_{-\infty}^{+\infty} H^{LT}_{ik,jl}(|\tilde{a}_{11}(t)|, \Omega) \times \tilde{a}_{jl}(\Omega) \times \frac{\tilde{a}_{jl}(t)}{\tilde{a}*_{jl}(t)} \times d\Omega \end{Bmatrix}, \quad (5)$$

$$+ \sum_{jl \neq 1,1} \begin{Bmatrix} T_{ik,jl}(|\tilde{a}_{11}(t)|) \times P^{k-l} \times \tilde{a}_{jl}(\Omega) \\ + \frac{1}{2\pi}\int_{-\infty}^{+\infty} H^{ST}_{ik,jl}(|\tilde{a}_{11}(t)|, \Omega) \times \tilde{a}_{jl}(\Omega) \times d\Omega \\ + \frac{1}{2\pi}\int_{-\infty}^{+\infty} H^{LT}_{ik,jl}(|\tilde{a}_{11}(t)|, \Omega) \times \tilde{a}_{jl}(\Omega) \times \frac{\tilde{a}_{jl}(t)}{\tilde{a}*_{jl}(t)} \times d\Omega \end{Bmatrix}.$$

with $P = e^{j(\tilde{a}_{11}(t))}$.

As a first iteration, the model is simplified to take into account only short-term memory effects. The kernel $H^{LT}_{ik,jl}$ is removed from the expression as it describes low-frequency memory effects. The expression of MHV model is described in [14] as (6)

$$\tilde{b}_{ik}(t) = \sum_{jl} \frac{1}{2\pi}\int_{-\infty}^{+\infty} S_{ik,jl}(|\tilde{a}_{11}(t)|, \Omega) P^{k-l} \tilde{a}_{jl}(\Omega) \times d\Omega + \sum_{jl} \frac{1}{2\pi}\int_{-\infty}^{+\infty} T_{ik,jl}(|\tilde{a}_{11}(t)|, \Omega) P^{k+l} \tilde{a}^*_{jl}(\Omega) \times d\Omega \quad (6)$$

with $P = e^{j\varphi_{\tilde{a}_{11}(t)}}$.

The topology of the model is described in Fig. 2.

The authors of [15] present an improved model which considers the coupled effects of short- and long-term memory within the pass-band region. According to (6), the $\tilde{b}_{21}(t)$ wave is linked to the contributions of $\tilde{a}_{1l}(t)$ and $\tilde{a}_{2l}(t)$, but for simplicity it is reduced to represent the overriding influence of $\tilde{a}_{11}(t)$. The resulting principle is represented by the feedback loop shown in Fig. 3.

The feedback loop consists of two basic nonlinear dynamics with widely separated time constants. The stronger of the nonlinear dynamics is the short-term response, responsible for the amplification and band-pass filtering effects of the amplifier (i.e., transistor transit time and matching network immittance profile). The weaker nonlinear dynamic is the long-term response; when a variable envelope signal traverses the feed-forward block, a portion of the output signal is fed back to the input. This long-term dynamic can be seen as slow modulation of the DC quiescent point of the amplifier resulting from the amplifier's thermal effects, trapping effects, and bias network low-pass filtering. We can extract the closed-loop equation (7) from Fig. 3, from which the approximation (8) is derived assuming the long-term contribution, $f_{LT}(|\tilde{a}_{11}(t)|, t)$ is reasonably small.

$$\tilde{b}_{21}(t) = \frac{f_{ST}(|\tilde{a}_{11}(t)|, t) \times \tilde{a}_{11}(t)}{1 - f_{LT}(|\tilde{a}_{11}(t)|, t) \times f_{ST}(|\tilde{a}_{11}(t)|, t)}, \quad (7)$$

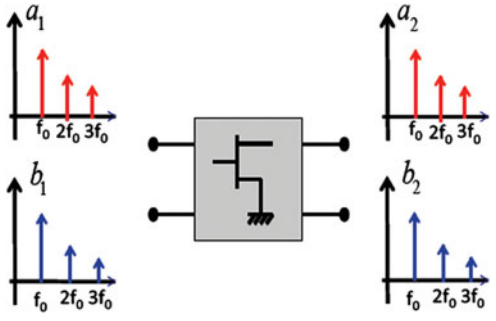

Fig. 1. Harmonic superposition principle.

https://doi.org/10.1017/S1759078713000068 Published online by Cambridge University Press

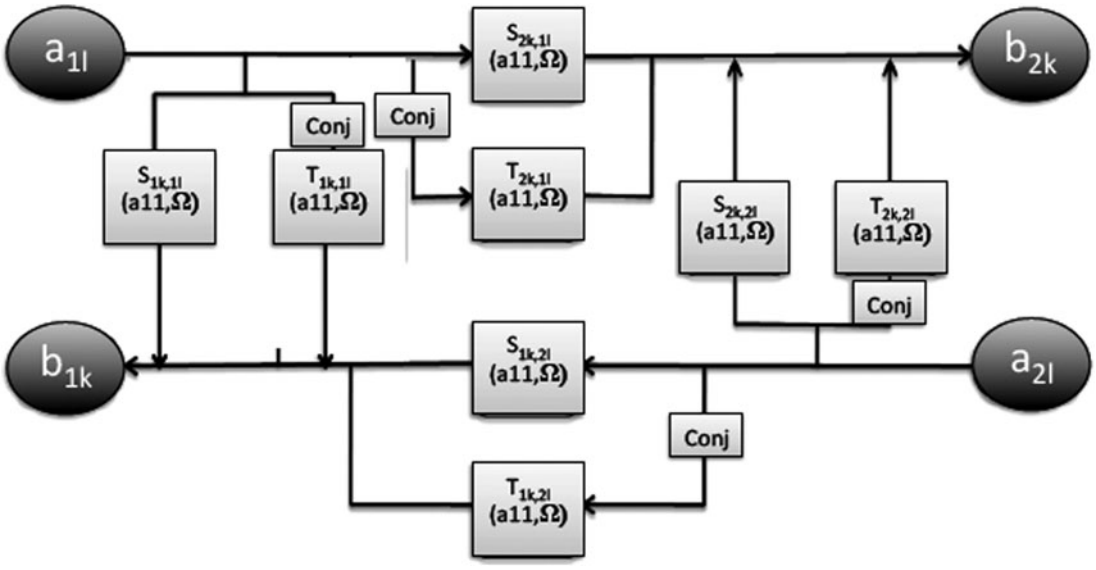

Fig. 2. Topology of the multi-harmonic Volterra model.

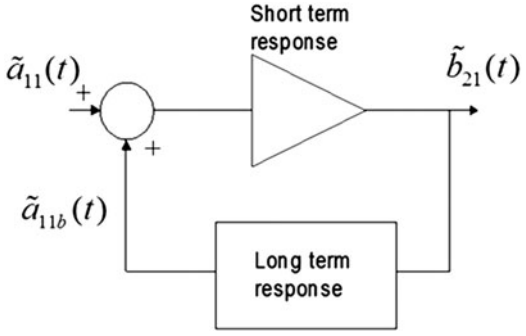

Fig. 3. Feedback loop principle.

$$\begin{aligned}\tilde{b}_{21}(t) &\cong \tilde{b}^{2}_{21}(t) \times \tilde{b}^{1}_{21}(t),\\ \tilde{b}^{1}_{21}(t) &= f_{ST}(|\tilde{a}_{11}(t)|, t) \times \tilde{a}_{11}(t),\\ \tilde{b}^{2}_{21}(t) &= 1 + f_{LT}(|\tilde{a}_{11}(t)|, t) \times f_{ST}(|\tilde{a}_{11}(t)|, t).\end{aligned} \tag{8}$$

Equation (8) defines the SSPA output $\tilde{b}_{21}(t)$ as the combination of $\tilde{b}^{1}_{21}(t)$and $\tilde{b}^{2}_{21}(t)$, where $\tilde{b}^{1}_{21}(t)$ is the amplifier's short-term response described by equation (6) and $\tilde{b}^{2}_{21}(t)$ is a modulating component containing both short-term and long-term dynamics. Because $\tilde{b}^{2}_{21}(t)$ depends only on the magnitude of the complex envelope signal and not on its phase, we can effectively describe it using the nonlinear impulse response model proposed in reference [16]; the response can be considered independent of the instantaneous frequency and written as

$$\tilde{b}^{2}_{21}(t) = 1 + \int_{0}^{\infty} \tilde{h}_{FB}(|\tilde{a}_{11}(t-\tau)|, \tau)|\tilde{a}_{11}(t-\tau)|d\tau. \tag{9}$$

Because of the index $j, l = 1, 1$ the T term can be removed from the general expressions (5) and (6) of $\tilde{b}^{1}_{21}(t)$. Finally, from (6, 8, and 9), we reformulate the SSPA output as

$$\begin{aligned}\tilde{b}_{21}(t) &= \tilde{b}^{2}_{21}(t) \times \tilde{b}^{1}_{21}(t),\\ \tilde{b}^{1}_{21}(t) &= \frac{1}{2\pi}\int_{-\infty}^{+\infty} S^{ST}_{2111}(|\tilde{a}_{11}(t)|, \Omega) \times \tilde{a}_{11}(\Omega) \times e^{j\times\Omega\times t} \times d\Omega,\\ \tilde{b}^{2}_{21}(t) &= 1 + \int_{0}^{\infty} S^{FB}_{2111}(|\tilde{a}_{11}(t-\tau)|, \tau)|\tilde{a}_{11}(t-\tau)|d\tau.\end{aligned} \tag{10}$$

From equation (10), the proposed model can be represented as the simple feed forward structure shown in Fig. 4. This diagram is similar to the one previously adopted in [17–19]; however, the novelty lies in the equations used to describe the two branches. These equations lead to a kernel extraction process which does not require an optimization process and thus guaranties solution uniqueness.

With regard to the multi-harmonic behavior of a nonlinear device, the model can be generalized as

$$\tilde{b}_{ik}(t) = \tilde{b}^{ST}_{ik}(t) \times \tilde{b}^{FB}_{ik}(t),$$

$$\tilde{b}^{ST}_{ik}(t) = \sum_{jl}\left\{\begin{array}{l}\frac{1}{2\pi}\int_{-\infty}^{+\infty} S^{ST}_{ik,jl}(|\tilde{a}_{11}(t)|, \Omega)\times\tilde{a}_{jl}(\Omega) \times d\Omega\\ +\frac{1}{2\pi}\int_{-\infty}^{+\infty} T^{ST}_{ik,jl}(|\tilde{a}_{11}(t)|, \Omega)\times\tilde{a}_{jl}(\Omega) \times \frac{\tilde{a}_{jl}(t)}{\tilde{a}^{*}_{jl}(t)} \times d\Omega\end{array}\right\}, \tag{11}$$

$$\tilde{b}^{FB}_{ik}(t) = \sum_{jl} 1 + \int_{0}^{\infty} S^{FB}_{ik,jl}(|\tilde{a}_{11}(t-\tau)|, \tau)\big|\tilde{a}_{jl}(t-\tau)\big|d\tau.$$

https://doi.org/10.1017/S1759078713000068 Published online by Cambridge University Press

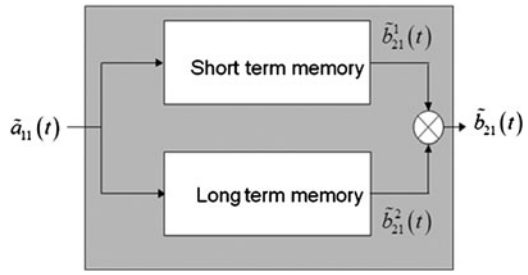

Fig. 4. New kernel topology.

III. EXTRACTION METHOD

A) Extraction method of short-term kernels

First, the short-term kernel $S_{2111}^{ST}(|\tilde{a}_{11}(t)|, \Omega)$ is unambiguously identified by driving the amplifier with a single tone signal where the component $\tilde{b}_{ik}^{LT}(t) = 1$, $|\tilde{a}_{11}(t)|$ being time independent. To better understand the model extraction methodology, the equation of b_{21} for a two-harmonic model example is described as

$$\begin{aligned}\tilde{b}_{21} = {} & S_{21,11}(|\tilde{a}_{11}|, \Omega).\tilde{a}_{11} + S_{21,12}(|\tilde{a}_{11}|, \Omega).\tilde{a}_{12} \\ & + S_{21,21}(|\tilde{a}_{11}|, \Omega).\tilde{a}_{21} + S_{21,22}(|\tilde{a}_{11}|, \Omega).\tilde{a}_{22} \\ & + T_{21,11}(|\tilde{a}_{11}|, \Omega).\tilde{a}_{11}^{*} + T_{21,12}(|\tilde{a}_{11}|, \Omega).\tilde{a}_{12}^{*} \\ & + T_{21,21}(|\tilde{a}_{11}|, \Omega).\tilde{a}_{21}^{*} + T_{21,22}(|\tilde{a}_{11}|, \Omega).\tilde{a}_{22}^{*}.\end{aligned} \tag{12}$$

The extraction of each pair of S and T parameters can be achieved by using one of the two methods. The first method is provided by AGILENT using the PNA-X in order to extract the X-parameters™ of the amplifier. It consists of adding a "tickle tone" to the large-signal tone at all harmonic frequencies. As described in [11], the theorem of harmonic superposition is used to solve the system. Moreover, it is important to note that both the power and the envelope frequency (Ω) are swept.

The second method involves setting the a-waves to zero, as done with S-parameter measurements, so that only a single pair of S and T terms will remain. In a two-harmonic example, only the b_2 wave is considered, while a_{21}, a_{12} and a_{22} are set to zero in order to extract the $S_{21,11}$ and $T_{21,11}$ terms. Harmonic load pull can be used to control impedances at both fundamentals and harmonic frequencies thereby setting the a-waves to zero in accordance with the reference impedance. This method is well suited for high-power amplifier or transistor characterization.

B) Extraction method of feedback kernels

The feedback kernels $S_{ik,jl}^{FB}(|\tilde{X}|, t)$ are determined by driving the amplifier with a unit-step envelope at the center frequency of the amplifier bandwidth. Dividing the amplifier output by the short-term response results in a signal $b_{ik,jl}^{2}(t)$ from which the impulse response $S_{ik,jl}^{FB}(|\tilde{X}|, t)$ is easily extracted. It is important to note that the driving signal $S_{ik,jl}^{FB}(|\tilde{X}|, t)$ corresponds directly to the time derivative of the output $\tilde{b}_{ik,jl}^{2}(t)$.

Pulse profiling is performed at the center frequency of the amplifier bandwidth for each load impedance state. This method assumes that identifying the short- and long-term coupling effects at the center frequency is sufficient for proper representation of the behavior of the device without the need for larger sets of data.

C) Model implementation

Vector Fit™ software is used to extract the frequency dependencies of all S and T parameters, and an iterative process is used to identify the minimum set of poles and residues. This description uses separate variables and is convenient for model implementation in commercial software. The relationship can be written as:

$$S_{ik,jl}(|\tilde{a}_{11}|, \Omega) = \sum_{n=1}^{N} \frac{r_{ik,jl}^{n}(|\tilde{a}_{11}|, \Omega)}{j\Omega - p_{ik,jl}^{n}}. \tag{13}$$

The user-compiled model, along with the R and C discrete elements, are introduced into ADS, where simulation can be carried out using both harmonic balance and envelope transient methodologies.

IV. MEASUREMENT AND SIMULATION RESULTS

Consider a Bipolar-Complementary Metal Oxide Semiconductor (BiCMOS) Low-Noise Amplifier (LNA) operating at 1.96 GHz containing an automatic gain control (AGC) loop, making it very sensitive to long-term memory effects. The CW gain compression plot of the LNA at the center frequency 1.96 GHz is given in Fig. 5.

Figure 6 shows the real and imaginary parts of the short-term kernel $S_{21,11}^{ST}(|\tilde{a}_{11}(t)|, \Omega)$ over a 400 MHz bandwidth.

Figure 7 shows the real and imaginary parts of the feedback kernel $1 + \int_0^{\infty} S_{21,11}^{FB}(|\tilde{a}_{11}(t-\tau)|, \tau)$. A long transient duration of about 10 μs is observed.

The extracted model was tested with a 16-Quadrature amplitude modulation (QAM) modulated signal with 2 MB/s and 40 MB/s bit rates. Figures 8 and 9 compare the model predictions with the results obtained from a transistor-level simulation.

The agreement between the models and the circuit simulations are quite good, generally within a few dB. In comparison, the classical X-parameter model deviated by as much as 15 dB. It is important to remark that the main advantage of the MHV model compared with [13] is its ability to provide good predictions at high modulation rates due to the integration of the short-term memory. Additionally, it is important to note that the model simulation time is only several minutes, while the circuit simulation required several hours.

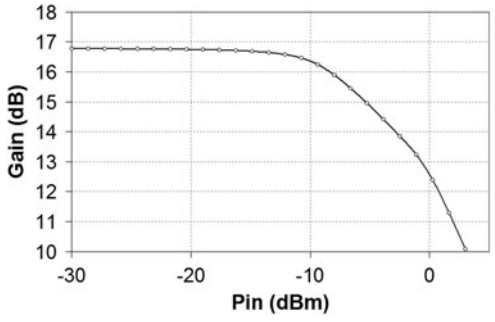

Fig. 5. CW gain compression versus input power.

https://doi.org/10.1017/S1759078713000068 Published online by Cambridge University Press

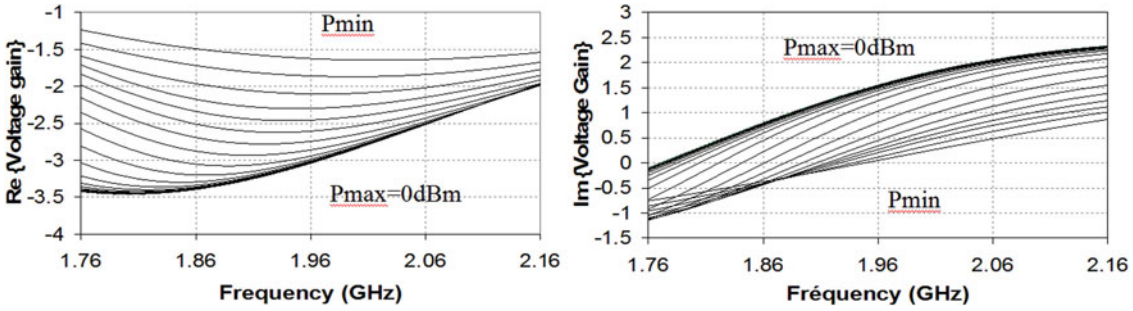

Fig. 6. Transfer function $S^{ST}_{21,11}(|\tilde{a}_{11}(t)|, \Omega)$.

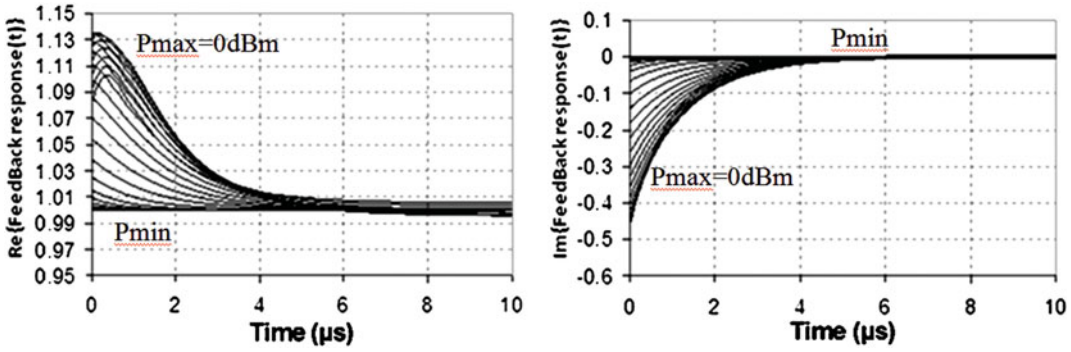

Fig. 7. Extraction results of feedback kernel.

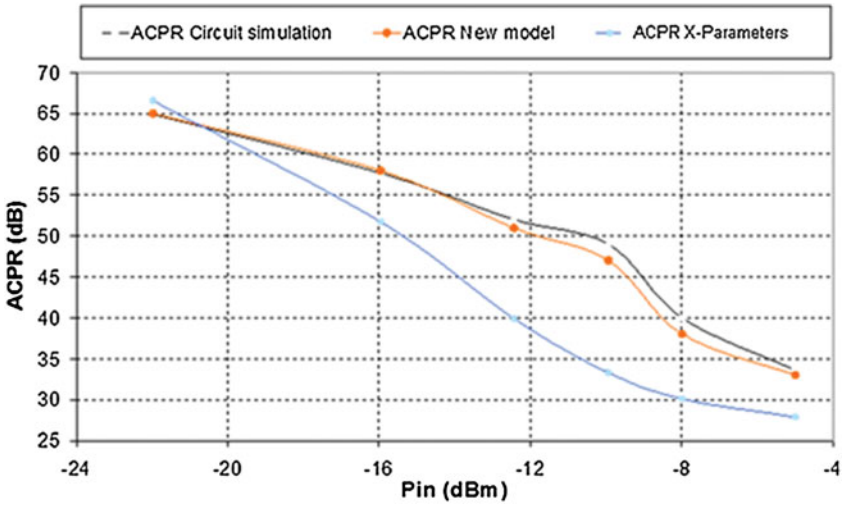

Fig. 8. ACPR = f(Pin) 16-QAM at 2 MB/s.

Consider a three-stage Heterostructure Field Effect Transistor (HFET) power amplifier operating at 1.6 GHz. Using the second extraction method described in Section III.1, harmonic load pull was used to control impedances at both fundamentals and harmonic frequencies, thereby setting the a-waves to zero. The PNA-X NVNA measured the $\tilde{a}_{jl}$ and $\tilde{b}_{ik}$ parameters for varying $\tilde{a}_{jl}$. Figure 10 shows the setup used in the model extraction.

The nonlinear long-term time constant of about 200 µs is highlighted by the plot of the extracted feedback kernel $1 + \int_0^\infty S^{FB}_{2111}(|\tilde{a}_{11}(t-\tau)|, \tau)$, Fig. 11.

The extracted model was tested with a 16-QAM modulated signal and 10 MB/s bit rate. Figure 12 compares the waveforms of measured $\tilde{b}_{21}$, the MHV modeling approach and classical X-parameters. The corresponding values of EVM are 2.3% (measurements) 3.0% (MHV model simulation), and 7.2% (classical X-parameters). These results were obtained at a fixed fundamental load impedance of 65 Ω while 2fo and 3fo were set to 50 Ω.

Additionally, C/I measurements were performed using a narrow bandwidth signal (from 10 kHz to 5 MHz) in order to verify the model's long-term memory-effect prediction capabilities.

The new model provides a significant accuracy improvement compared with a classical memoryless model, which does not take into account frequency spacing of two-tone

https://doi.org/10.1017/S1759078713000068 Published online by Cambridge University Press

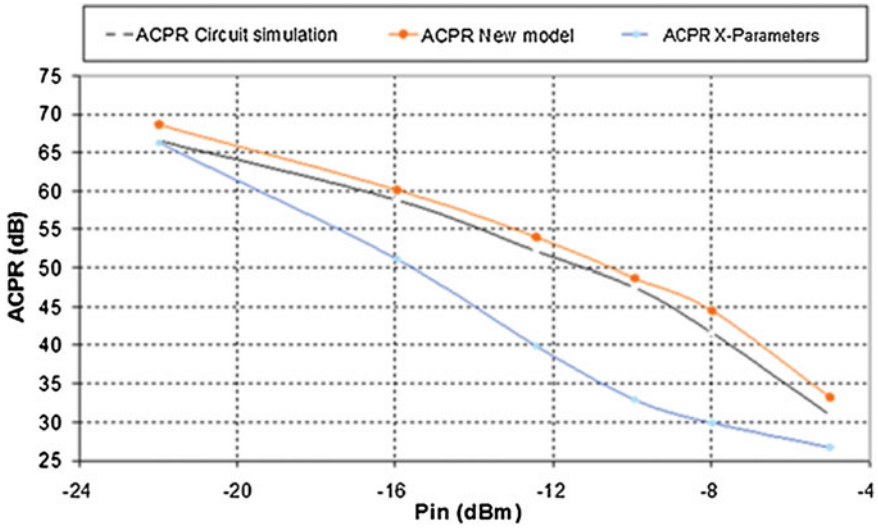

Fig. 9. ACPR = f(Pin) 16-QAM at 40 MB/s.

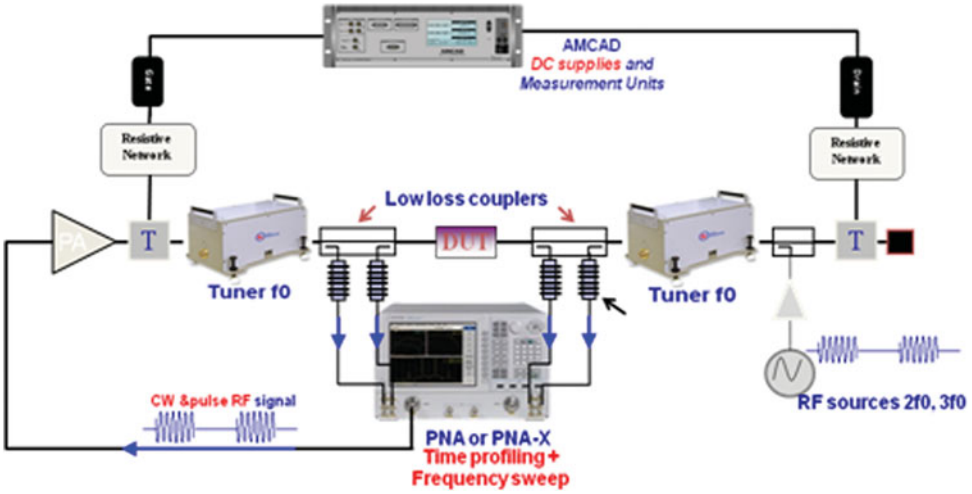

Fig. 10. AMCAD setup for behavioral model extraction.

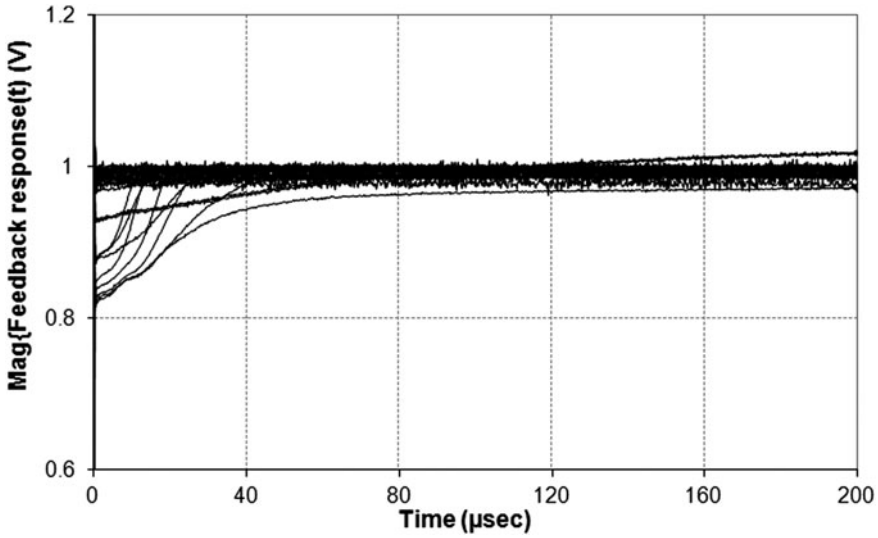

Fig. 11. Extraction results of feedback kernel.

https://doi.org/10.1017/S1759078713000068 Published online by Cambridge University Press

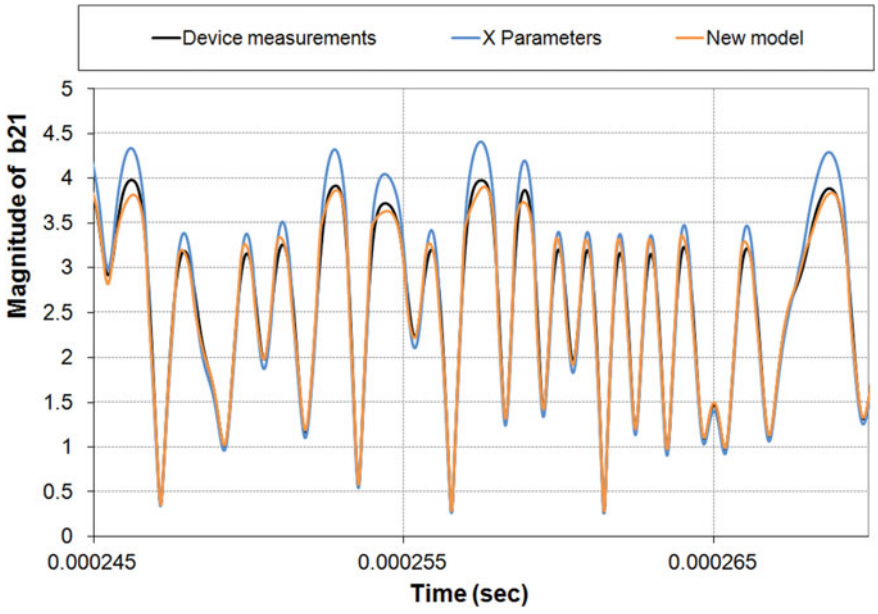

Fig. 12. Time-domain envelope.

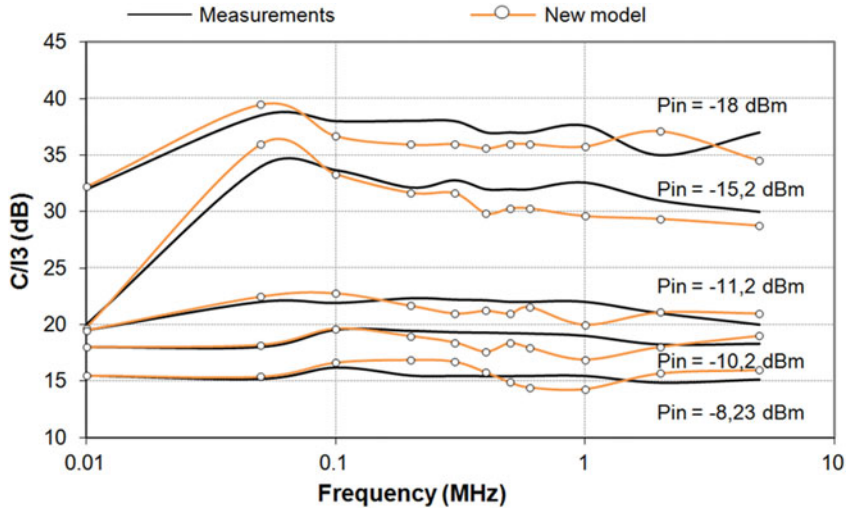

Fig. 13. C/I3 measurements versus simulation.

signals. Using this new model, C/I3 can be predicted with an error <2 dB across power and tone spacing (Fig. 13).

IV. CONCLUSION

An efficient new dynamic mapping technique based on Volterra expansion has been proposed. It has been successfully proven that this model can accurately reproduce the nonlinear envelope distortions under low mismatched conditions. The proposed model extraction is straightforward for both circuit-level simulation and time-domain envelope measurements. The extraction principle does not require a parameter optimization process. The model can be extended to predict DC consumption, which is a critical parameter for power amplifiers and system link budgets.

ACKNOWLEDGEMENTS

AMCAD Engineering would like to thank Mr. Gustavsen for providing Vector-Fit software, as well as Agilent Technologies for the latest Agilent ADS software. AMCAD Engineering would like also to thank the Catrene project 101 "PANAMA" for the support and Steve Dudkiewicz for the reviewing.

REFERENCES

[1] Saleh, A.: Frequency-independent and frequency-dependent nonlinear models of TWT amplifiers. IEEE Trans. Commun., **COM-29** (1981), 1715–1720.

[2] Abuelma'atti, M.: Frequency-dependent nonlinear quadrature model for TWT amplifiers. IEEE Trans. Commun., **COM-29** (1984), 982–986.

https://doi.org/10.1017/S1759078713000068 Published online by Cambridge University Press

[3] Silva, C.P.; Aerosp. Corp., El Segundo, C.A.; Clark, C.J.; Moulthrop, A.A.; Muha, M.S.: Optimal-filter approach for non linear power amplifier modelling and equalization, in IEEE MTT-S Int. Microwave Symp. Dig, Boston, MA, June 2000, 437–440.

[4] Silva, C.P.; Moulthrop, A.A.; Muha, M.S.: Introduction to polyspectral modeling and compensation techniques for wideband communications systems, in 58th ARFTG Conf. Dig., San Diego, CA, November 2001.

[5] Pedro, J.C.; Carvalho, N.B.; Lavrador, P.M.: Modeling nonlinear behavior of band-pass memoryless and dynamic systems, in IEEE MTT-S Int. Microwave Symp. Dig.-CDROM, Philadelphia, PA, June 2003.

[6] Ku, H.; Kenney, J.S.: Behavioral modeling of RF power amplifiers, in IEEE MTT-S Int. Microwave Symp. Dig.-CDROM, Philadelphia, PA, June 2003.

[7] Zhu, A.; Wren, M.; Brazil, T.J.: An efficient Volterra-based bahavioral model for wideband RF power amplifiers, in IEEE MTT-S Int. Microwave Symp. Dig.-CDROM, Philadelphia, PA, June 2003.

[8] Filicori, F.; Vannini, G.; Monaco, V.A.: A non linear integral model of electron devices for HB analysis. IEEE Trans. Microw. Theory Tech., **MTT-40** (1992), 1456–1465.

[9] Mirri, D.; Filicori, F.; Iuculano, G.; Pasini, G.: A non-linear dynamic model for performance analysis of large-signal amplifier in communication systems, in IMTC/99 IEEE Instrumentation and Measurement Technology Conf. Dig, Venice, May 1999, 193–197.

[10] Le Gallou, N.; Ngoya, E.; Buret, H.; Barataud, D.; Nebus, J.M.: An improved behavioral modeling technique for high power amplifiers with memory, in IEEE MTT-S International Microwave Symp. Dig., Phoenix, AZ, 2001, 983–986.

[11] Verspecht, J.; Root, D.: Polyharmonic distortion modeling. IEEE Microwav. Mag., **7** (3) (2006), 44–57.

[12] Horn, J.M.; Verspecht, J.; Gunyan, D.; Betts, L.; Root, D.E.; Eriksson, J.: X-parameter measurement and simulation of a GSM handset amplifier, in IEEE 3rd EUMIC Conf. EUMW, Amsterdam, 2008.

[13] Soury, A.; Ngoya, E.: Handling long-term memory effects in X-parameters model, in IEEE MTT-S Int. Microwave Symp. Dig.-CDROM, Montréal, Canada, June 2012.

[14] Demenitroux, W.; Maziere, C.; Gasseling, T.; Gustavsen, B.; Campovecchio, M.; Quere, R.: A new multi-harmonic and bilateral behavioral model taking into account short term memory effect, in Microwave Conf. EuMC, Paris, October 2010, 473–476.

[15] Maziere, C.; Soury, A.; Ngoya, E.; Nebus, J.M.: A system level model of solid state amplifiers with memory based on a non linear feedback loop principle, in IEEE 8th European Conf. Wireless Technology – European Microwave Week 2005, Paris, October 2005.

[16] Bennadji, A.; Layec, A.; Soury, A.; Mallet, A.; Ngoya, E.; Quere, R.: Modeling of a communication chain with implementation of a Volterra power amplifier model for efficient system level simulation, in IEEE 8th European Conf. Wireless Technology – European Microwave Week 2005, Paris, October 2005.

[17] Bosch, W.; Gatti, G.: Measurement and modeling techniques for wideband communication components and systems. Int. J. RF Microw. Comput. Aided Eng. (USA), **13** (1) (1989), 5–31.

[18] Meghdadi, V.: Modeling of solid state power amplifier (SSPA) and validation by means of a system simulator. Ann. Telecommun. (France), **53** (1–2) (1998), 4–14.

[19] Draxler, P.; Langmore, I.; Hung, T.P.; Asbeck, P.M.: Time domain characterization of power amplifiers with memory effects, in IEEE MTT-S Int. Microwave Symp. Dig.-CDROM, Philadelphia, PA, June 2003.

Christophe Mazière was born in Limoges, France, in 1977. He received the M.S. and Ph.D. degrees in electrical engineering from the University of Limoges, respectively, in 2001 and 2004. His research work deals with behavioral modeling of nonlinear devices. In 2006, he joined AMCAD Engineering where he works on the development of advanced test benches for high power devices' characterization. Since 2009, he developed the activity of behavioral modeling with multi-harmonics models.

Emmanuel Gatard received the electronics and telecommunications engineering degree from ENSIL, Limoges, France and the Ph.D. degree in electrical engineering from the University of Limoges, in 2006. His research interests at the XLIM research laboratory was electrothermal modeling of power semiconductor devices dedicated to circuit simulations, physics-based electron device simulations, and nonlinear thermal modeling. Since 2008, he joined AMCAD engineering where he is in charge of development of advanced test benches for high power devices' characterization. He also works on envelope tracking amplifiers and MEMS switches modeling.

Cédric Enguehard received his Ph.D. degree in 2011. The subject of his research was the study of differential structures for RF low noise amplifiers at XLIM laboratory in Limoges. During his Ph.D. he was involved in MMIC design of Low Noise Differential Amplifier, MMIC Si devices, and RF advanced measurements. He joined AMCAD engineering in 2012 and is currently in charge of RF and microwave measurement.

Bjørn Gustavsen received the Dr. Ing. degree in electrical engineering from the Norwegian Institute of Technology (NTH) in Trondheim, Norway, in 1993. Since 1994 he has been working at SINTEF Energy Research where he is the Chief Research Scientist. His interests include simulation of electromagnetic transients and modeling of frequency-dependent effects. He spent 1996 as a Visiting Researcher at the University of Toronto, Canada. He was a Marie Curie Fellow at the University of Stuttgart, Germany, between August 2001 and August 2002.

https://doi.org/10.1017/S1759078713000068 Published online by Cambridge University Press